Full paper/Mémoire

A novel magnetic biosorbent prepared using an oak shell waste material as an efficient adsorbent for consecutive removal of Pb^{2+}, Ag^+, Ba^{2+}, Sr^{2+}, and CrO_4^{2-} from aqueous solutions

Maryam Adibmehr, Hossein Faghihian[*]

Department of Chemistry, Shahreza Branch, Islamic Azad University, P.O. Box 311-86145, Shahreza, Iran

ARTICLE INFO

ABSTRACT

In this research, the performance of a new biosorbent prepared using low-cost oak shell waste materials for consecutive removal of particular cations and chromate anions from aqueous solutions was studied. The adsorbent impregnated with Pb^{2+}, Ag^+, Ba^{2+}, and Sr^{2+} was used to remove chromate anions by the formation of an appropriate insoluble precipitate. The biosorbent was characterized by FTIR, XRD, SEM, TG-DTG, and VSM techniques. The adsorption capacities of 133.84, 53.12, 50.12, and 40.39 mg g^{-1} were obtained for chromate for the samples containing Pb^{2+}, Ag^+, Ba^{2+}, and Sr^{2+} cations, respectively. The chromate uptake was inversely proportional to the k_{sp} of the chromate precipitate and increased with the cation content of the adsorbent. The adsorption process was kinetically fast and the equilibrium was established within 10 min. The experimental data were analyzed by the Langmuir, Freundlich, Sips, and Redlich-Peterson isotherm models. The data were fitted to the Langmuir isotherm, indicating that chromate was adsorbed homogeneously on the adsorbent surface.

© 2018 Académie des sciences. Published by Elsevier Masson SAS. All rights reserved.

1. Introduction

With increasing industrial activities, a large amount of waste and run-off from the industries enters the environment and causes serious health problems. Chromium is one of the hazardous element that is widely released into the environment from leather tanning, cement, plastic, metallurgical, textile, batteries, refractories, pigment, welding, stainless steel, ceramic, catalysis, wood preservatives, electroplating, photography, galvanometric, metal cleaning, and mining industries [1,2]. Although chromium has several oxidation states, from −2 to +6, Cr(VI) it is more soluble, toxic, carcinogenic, and non biodegradable. Moreover, as a mutagenic agent, it causes serious health problems such as dermatitis, allergic sensitization, stomachache, nausea, vomiting, severe diarrhea, hemorrhage, epigastric pain liver, kidney and respiratory damages, and gastrointestinal ulcers [3–5]. Based on the pH of the solutions, Cr(VI) exists as different species such as chromates (CrO_4^{2-}), dichromates ($Cr_2O_7^{2-}$), and bichromates ($HCrO_4^-$) [6].

Various conventional techniques have been employed to remove chromium from wastewaters including precipitation [7], ion exchange [8], ultrafiltration [9], flotation [10], reverse osmosis [11], electrochemical [12], and coagulation [13]. These methods generally suffer from disadvantages such as cost, production of chemical sludge [14], and harmful chemicals as a secondary pollutant [15]. Adsorption is the most favorite and feasible technique for the separation of pollutants owing to its high efficiency, selectivity, low-cost, and easy handling [16].

* Corresponding author.
   E-mail address: faghihian@iaush.ac.ir (H. Faghihian).

Different adsorbents such as resins [17], goethite [18], zeolite [19], MCM-41 [20], clay [21], and gamma Al_2O_3 [22] have been employed for the removal of chromates. The use of biosorbents has been enhanced in recent days in plant species such as walnut shells [23], pine cone [24], oak shell [25], and maize spatha [26].

Nevertheless, many concerns have arisen for the discharge of toxic metals from industries into the environment such that intensive studies are underway to develop cost-effective adsorbents using environmentally friendly biomaterials for the removal of heavy metals from liquid wastes.

Many researchers developed production of activated carbons to reduce the preparation cost of the adsorbent. Activated carbons (AC) have unique properties such as high porosity, large surface areas, and functionalized surface. They are prepared economically and their efficiency can be readily improved via the chemical modification [27,28]. Although the reactivity of the nano-sized adsorbents is higher than their micro-sized counterparts, their separation from the solution is incomplete, tedious, and time-consuming. One way to eliminate the separation difficulties is to consider the magnetization of adsorbents by iron oxide.

In this research, a biosorbent was prepared using an oak shell obtained from local agricultural waste materials. It was magnetized using Fe_3O_4, functionalized with dithizone, and then impregnated with particular cations. The cation-loaded adsorbents were used for the removal of chromate anions from aqueous solutions under different experimental conditions.

2. Experimental

2.1. Materials and methods

Analytical grade reagents were provided from Merck Company. Stock solutions of cations were prepared by dissolving appropriate amount of nitrate salt in de-ionized water. The chromium stock solution was prepared by dissolving accurately weighed amount of potassium dichromate into deionized water. Characterization of the samples was performed by using different techniques including a scanning electron microscope (MIRA3LMU model, TESCAN Company), X-ray diffraction system (PANalytical model X'Pert PRO), Fourier transforms infrared spectrometer (FTIR Perkin–Elmer 65), and thermal analyzer (TG-DTG) (NETZSCH STA 409 PC/PG), VSM (LDJ Electronics Inc., Model 9600). The concentration of cations was measured using an atomic absorption spectrometer (Shimadzu Elmer Perkin devices 300 Analyst model A). Chromate concentration was measured using the HPLC method by using an Agilent Technologies 1200 Series instrument with a Quaternary pump, column XDB-C18 ($L = 25$ cm, id $= 4.6$ mm and particle size$= 5$ μm, Injected and detected volumes: 5 μL, flow rate: 1 mL min^{-1}).

2.2. Preparation, magnetization and functionalization of activated carbons

Activated carbon (AC) was prepared by the carbonization of oak shell waste materials collected from Zagros

forests, Kohmareh Sorkhi region, Fars, Iran. The process was executed in a quartz tube furnace under a N_2 atmosphere. The AC was then treated, respectively, with hydrochloric acid, and nitric acid to remove remaining organic matters and to increase the surface functional groups. The acid treated sample was denoted as AC-COOH. The acid treated AC was magnetized using Fe_3O_4 nanoparticles synthesized in the presence of activated carbon under alkaline conditions and inert atmosphere. 0.21 g of $FeSO_4 \cdot 7H_2O$ and 0.31 g of $FeCl_3 \cdot 6H_2O$ were dissolved in 8.0 mL of de-ionized water and 1.0 mL of ammonium hydroxide solution (25%, w/v) was added dropwise to the solution. 1.0 g of AC–COOH was then added and the mixture was vigorously stirred for 30 min at 80 °C. The mixture was cooled down to room temperature and the solid was removed and washed repeatedly with distilled water until the pH of filtrate was 5–6. The magnetized activated carbon (AC–Fe_3O_4) was dried and stored in desiccators [29]. To increase the selectivity and capacity of the adsorbent, the magnetic adsorbent was functionalized using dithizone. For functionalization, AC-Fe_3O_4 was first reacted with thionyl chloride to produce acyl chloride (AC-COCL) which then was reacted with dithizone solution. The functionalized adsorbent (AC-Fe_3O_4-DTZ) was magnetically separated, thoroughly washed with DMF, ethanol and diethyl ether, respectively, and dried at 70 °C for 8 h [25,30].

2.3. Confinement of AC-Fe_3O_4-DTZ with Pb^{2+}, Ag^+, Ba^{2+} and Sr^{2+} cations

To study the performance of AC-Fe_3O_4-DTZ for consecutive removal of the studied cations and chromate anions, the adsorption capacity of the sorbent towards the cations was firstly measured, and then the cation-loaded adsorbents were employed for the removal of chromate from aqueous solutions. To evaluate the capability of the adsorbent for the uptake of cations, in a series of experiments 0.1 g of the functionalized adsorbent was equilibrated with 25 mL of Pb^{2+}, Ag^+, Ba^{2+}, Sr^{2+} solutions having different concentrations (100–5000 mg L^{-1}). The pH of the solution was adjusted to 6.5 and the mixture was shaken for 7 min until the equilibrium was established. The adsorbent was separated by a magnet bar placed outside of the reaction vessel and the concentration of the cation in the remaining solution was measured by an atomic absorption method. The amount of the adsorbed cation was calculated by the following equation:

$$Q = \frac{(C_0 - C_e) \times V}{m} \qquad (1)$$

where Q is the equilibrium adsorption capacity (mg g^{-1}), C_0 is the initial concentration of the metal ion (M), C_e is the equilibrium concentration (mg L^{-1}), V (L) is the volume of the solution, and m (g) is the mass of adsorbent. For each cation, four samples with different cation contents were prepared and denoted accordingly (Table 1). As indicated in Fig. S2, the adsorption capacity of the functionalized adsorbent towards the studied cation was higher than the other adsorbents. Therefore, the magnetized activated

carbon functionalized with dithizone (AC-Fe$_3$O$_4$-DTZ) was selected for cation loading and for successive chromate adsorption.

2.4. Chromate adsorption

The cation-loaded adsorbents prepared in the previous section were employed for the adsorption of chromate from aqueous solutions. The adsorption performance of the samples towards CrO$_4^{2-}$ was examined by putting known amount (0.7, 1.7, 1.8 and 2.2 g) of each biosorbent confined with Pb^{2+}, Ag$^+$, Ba^{2+}, Sr^{2+} in contact with 25 mL of chromate solutions. The mixture was shaken for 10 min, the adsorbent was magnetically removed and the chromate concentration in the remaining solution was measured by a HPLC method. The effect of chromate concentration (100–5000 mg L^{-1}), contact time (3–14 min), adsorbent dose (0.1–2.6 g), and effect of pH (5–10) on the uptake of chromate was evaluated. The selectivity of the adsorbent in the presence of different anions was also studied. For each cation, four samples with different cation loadings were used.

3. Results and discussion

3.1. Characterization of the adsorbent

Characterization of the adsorbent was performed by the methods described in the previously published study [25]. In the FTIR spectrum of the AC sample, the adsorption band at 3435 cm^{-1} was attributed to the O–H stretching of water molecules and the peaks at 3038, 1798 and 1568 cm^{-1} were referred to C–H stretch, C=O stretch, and C=C stretch, respectively. The absorption bands at 1201 and 1252 cm^{-1} are referred to the =C–O asymmetric stretch. The peaks at 472, 713, 782 and 876 corresponded to the C–H bond. The band at 1026 was attributed to the C–O stretch (Fig. 1a).

In the FTIR spectrum of the AC-COOH sample, the absorption bands at 3072 and 3975 cm^{-1} referred to the O–H stretch. The band appeared at 2893 cm^{-1} corresponded to C–H stretching. Aromatic C=C ring stretching was

Table 1
Various samples with different cation loading.

Cation	Sample designation	Cation conc. (mg L^{-1})	Adsorbed cation (meq g^{-1})
Pb^{2+}	Pb-ads-1	50	0.11
	Pb-ads-2	100	0.23
	Pb-ads-3	1000	1.08
	Pb-ads-4	4000	2.44
Ag$^+$	Ag-ads-1	50	0.06
	Ag-ads-2	100	0.21
	Ag-ads-3	1000	0.47
	Ag-ads-4	4000	0.98
Ba^{2+}	Ba-ads-1	50	0.05
	Ba-ads-2	100	0.07
	Ba-ads-3	1000	0.44
	Ba-ads-4	4000	1.04
Sr^{2+}	Sr-ads-1	50	0.04
	Sr-ads-2	100	0.08
	Sr-ads-3	1000	0.08
	Sr-ads-4	4000	0.99

observed at 1432–1667 cm^{-1}. The peak at 1709 was attributed to the C=O stretch. The C–O stretch was appeared at 1062 and 1165 cm^{-1}. The bands at 610–700 cm^{-1} were assigned to the ≡C–H group (Fig. 1b).

In the FTIR spectrum of AC-Fe$_3$O$_4$-DTZ, the characteristic absorption bands appeared at 1706 and 1654 cm^{-1} corresponded to the stretching of the carbonyl group and the bands at 3745, 2877 and 1096 cm^{-1} belonged to the stretching of the hydroxyl group. The bands observed at 3323 and 1586 cm^{-1} were attributed to the stretch of –NH groups of amines and the bands at 1248 cm^{-1} corresponded to the stretch of C–N. The bands appeared at 1162 and 811 cm^{-1} assigned to the stretching of C–S and C=S, respectively. The Fe–O band appeared at 661 cm^{-1}. The characteristic bands of DTZ observed at 762, 1380, 1432, and 1529 cm^{-1} were attributed to the benzene ring stretching modes [31]. From the absorption bands appeared in the FTIR spectrum of the sample, it was concluded that dithizone was successfully immobilized on the surface of the biosorbent. The absorption band belonged to Fe–O was appeared at 573 cm^{-1} in the magnetic biosorbent (Fig. 1c).

From the SEM image of the acid treated activated carbon, it was obvious that the surface of the adsorbent was rough and highly porous with wide cavities and pores throughout the sample. This indicated that during the acid treatment, the impurities and soluble compounds were dissolved leading to the creation of wider and deeper pores and channels (Fig. 2).

In the SEM image of AC-Fe$_3$O$_4$-DTZ, due to the immobilization of Fe$_3$O$_4$ and dithizone on the surface of the adsorbent, the roughness of the surface was significantly decreased. The pore diameter of the samples was determined using Digmaizer software. The average pore diameters of AC-COOH and AC-Fe$_3$O$_4$-DTZ samples were, respectively, 29.8 and 13.5 μm.

The XRD patterns of AC-Fe$_3$O$_4$-DTZ represented in Fig. 3 showed that wide and strong background diffractions were appeared at 24 and 45° confirming the amorphous nature of the sample. The characteristic diffraction lines of dithizone at 8, 10, 15, 18, 20, 22, and 25° were properly overlapped by diffraction bands of activated carbon (Fig. 3d). The most intensive characteristic line of Fe$_3$O$_4$ at 37.5° (Fig. 3c) was also properly overlapped by the diffraction band of activated carbon [32,33]. The small peak at 60° was referred to Fe$_3$O$_4$. The other diffraction lines of Fe$_3$O$_4$ were covered by the second diffraction band of activated carbon. The EDAX analysis showed that the Fe$_3$O$_4$ content of the sample was about 1%, and lower than the detection limit of the XRD method, resulting the absence of some diffraction lines of this component.

The surface chemical composition of AC-Fe$_3$O$_4$-DTZ determined by EDAX is illustrated in Fig. S1. Carbon, nitrogen, oxygen, sulfur, and iron were recognized as the major constituent elements which are derived, respectively, from activated carbon, dithizone and Fe$_3$O$_4$. The elemental mappings indicated the uniform distribution of the element on the surface of the adsorbent (Fig. 4).

The magnetization curve of AC-Fe$_3$O$_4$-DTZ obtained using a Vibrating Sample Magnetometer (VSM) represented in Fig. 5. The magnetic properties of the sample
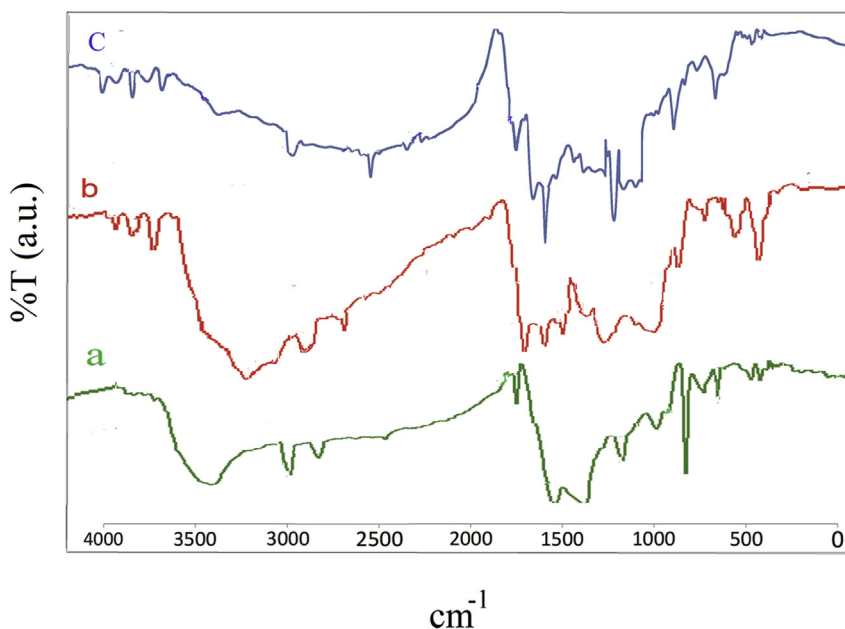
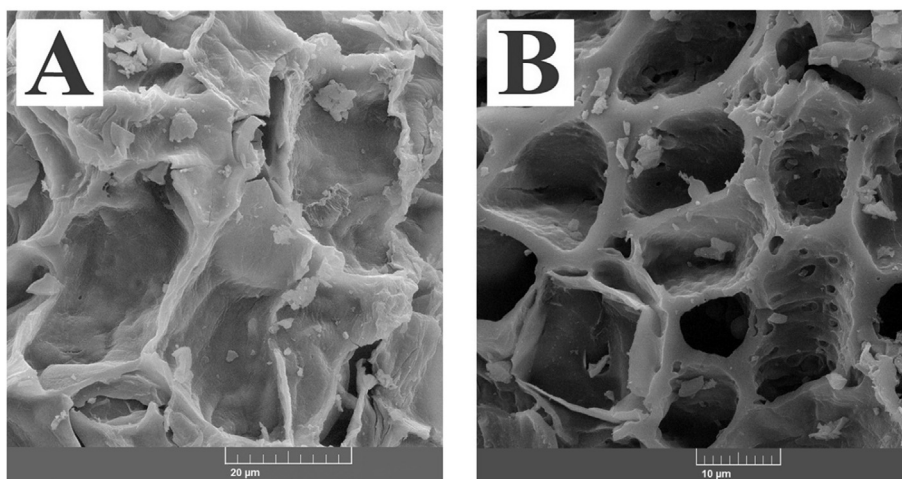**Fig. 1.** FTIR spectra of AC (a), AC-COOH (b) and AC-Fe$_3$O$_4$-DTZ (c).

Fig. 2. SEM images of activated carbons treated with HNO$_3$ (A) and AC-Fe$_3$O$_4$-DTZ sample (B).

were low (<10 emu g^{-1}) but as illustrated in the inset shows that the adsorbent was readily separated from the solution by putting a magnetic bar outside of the vessel. Other researchers working with magnetic composites reported that they also removed the composite from the solutions with magnetic properties lower than 10 emu g^{-1} [34]. In this research, after putting the magnet bar, separation of adsorbent was occurred in very short time and the particles were collected on the inside wall of the vessel. When the magnetic field was removed, the adsorbent dispersed homogeneously in the aqueous phase.

In the thermal curves (TG-DTG) of the sample taken under a nitrogen atmosphere, three well resolved weight loss peaks were distinguished (Fig. 6). The first weight loss

appeared between 100 and 200 °C was attributed to the evaporation of the adsorbed water molecules. The second weight loss step occurred between 300 and 420 °C and corresponded to the dehydration of hydroxyl groups and decomposition of the remaining organic constituents such as lignocellulosic [35]. The final weight loss step occurred above 600 °C and mainly involved the destruction of the dithizone structure [32].

3.2. Uptake of cations by the modified adsorbent

In the experiment performed with different adsorbents, the uptake of chromate was measured in three samples including activated carbon (AC), magnetized activated
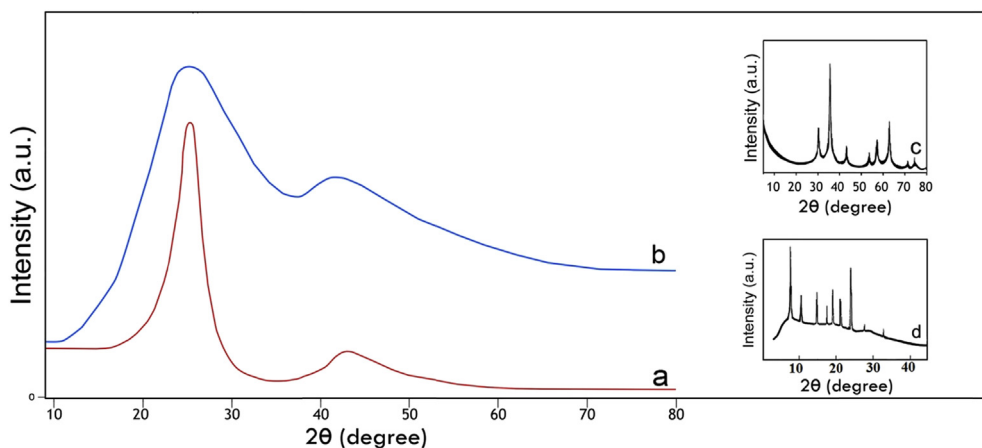
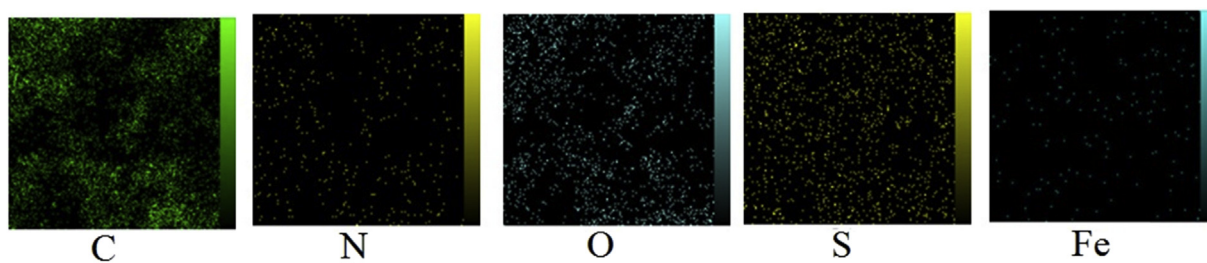**Fig. 3.** XRD patterns of AC (a), AC-Fe$_3$O$_4$-DTZ (b), Fe$_3$O$_4$ (c) and DTZ (d).

Fig. 4. Map of element of AC-Fe$_3$O$_4$-DTZ obtained by EDAX method.
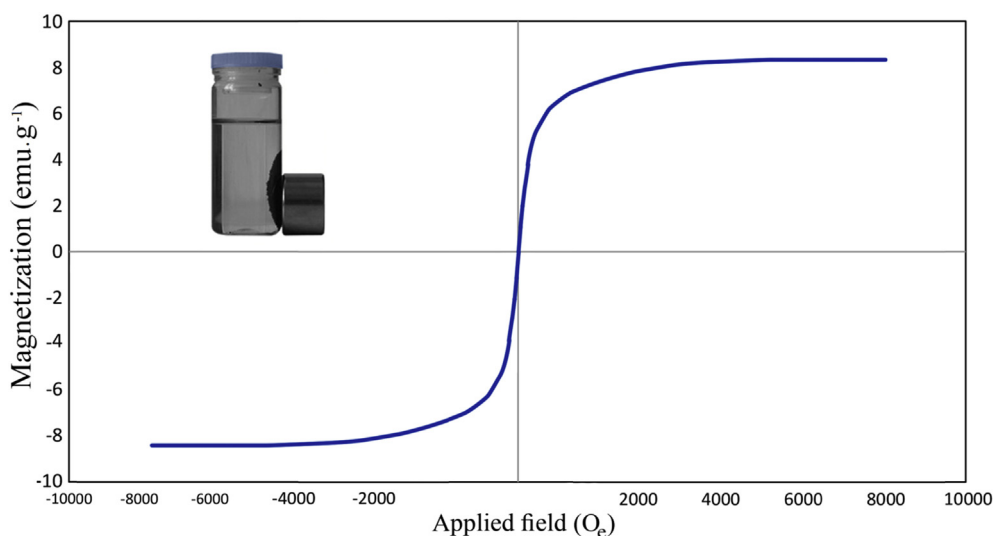
Fig. 5. VSM curve of AC-Fe$_3$O$_4$-DTZ.

carbon (AC-Fe$_3$O$_4$), and functionalized activated carbon (AC-Fe$_3$O$_4$-DTZ). The results (Fig. S2) showed that the adsorption of cations was in the order of AC-Fe$_3$O$_4$-DTZ>AC-Fe$_3$O$_4$> AC, suggesting that the introduction of Fe$_3$O$_4$ and dithizone into the activated carbon enhances its capacity toward the studied cations.

The basic idea behind this research is that the modified adsorbent is capable to adsorb particular cations from aqueous solutions, and then the adsorbents confined with cations can remove the chromate anion from the solution by the formation of appropriate insoluble chromate precipitate with the uploaded cations. To justify this
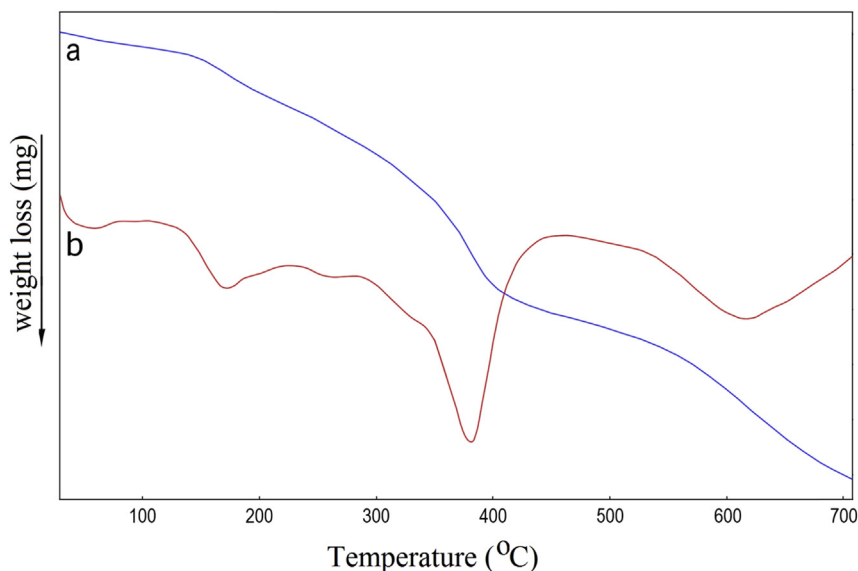
Fig. 6. Thermal curves TG (a) and DTG (b) of AC-Fe$_3$O$_4$-DTZ sample.

assumption, the modified biosorbents were firstly impregnated with Pb^{2+}, Ag$^+$, Ba^{2+}, and Sr^{2+} (the k_{sp} of PbCrO$_4$, Ag$_2$CrO$_4$, BaCrO$_4$, and SrCrO$_4$ is, respectively, 2.8 × 10^{-13}, 1.1 × 10^{-12}, 2.2 ×10^{-10}, and 2.2 ×10^{-05}) and the cation-loaded adsorbent was then used for the removal of chromate from solution.

By this method, the consecutive removal of selected cations and chromate ions by the same adsorbent from a single solution or different solutions is feasible.

To study the effect of the cation content on the removal efficiency of chromate, four adsorbents with different cation contents were prepared (Table 1). The maximum cation uptake for Pb^{2+}, Ag$^+$, Ba^{2+}, and Sr^{2+} was 2.44, 0.98, 1.04, and 0.99 meq.g^{-1}, respectively. The higher cation loading of Pb^{2+} is attributed to the higher affinity of the grafted ligand (dithizone) toward the lead ions. The high lead content is beneficial for the removal of chromate because the k_{sp} of lead chromate is very low (2.8× 10^{-13}) providing a favoring attracting force toward chromate ions. It is assumed that by selecting adequate ligands for each cation, it is possible to prepare new adsorbents with a higher cation content and to increase the removal efficiency of the adsorbent toward the chromate anion.

3.3. Removal of chromates by cation impregnated adsorbents

The chromate adsorption capacity of the adsorbent without cation loading was very limited (Fig. 7). By loading the cations into the biosorbent (AC–Fe$_3$O$_4$–DTZ), the uptake of chromate was increased and, for a particular cation, the increase was proportional to the cation content (Fig. 7). For the sample containing divalent cations (Pb^{2+}, Sr^{2+}, and Ba^{2+}) with almost similar cation content (Pb-ads-3,Ba-ads-4, and Sr-ads-4), the chromate uptake increased with a decrease in the k_{sp} of the chromate precipitate (Table 2).

For lead and silver loaded adsorbents, the adsorbed chromate was stoichiometrically equivalent to the Pb and Ag contents (Pb-ads-4 contained 2.44 meq g^{-1} of lead,

adsorbed 2.42 meq g^{-1} of chromate and Ag-ads-4 containing 0.980 meq g^{-1} of Ag, adsorbed 0.480 meq g^{-1} of chromate).

The adsorption of chromate in Ba-ads-4 and Sr-ads-4 was lower than the equivalent amount of the sorbed cations because the k_{sp} of their chromate precipitates was not sufficiently low and thus the tendency to the chromate attraction was insufficient. However, the results indicated that chromate adsorption was dependent on the cation content and the k_{sp} of the chromate precipitates.

4. Effect of experimental parameters on the chromate uptake

4.1. Effect of chromate concentration

The effect of chromate concentration on the removal efficiency was examined in the concentration range of 100–5000 mg L^{-1} (Fig. 7). It was found that the adsorption of chromate by the modified biosorbents increased with increasing chromate concentration until the adsorption sites were fully engaged and the equilibrium was established. By increasing the chromate concentration, the migration of chromate from the bulk solution to the surface of the adsorbent was enhanced and a higher uptake of the anion was achieved. The uptake of chromate has been studied using various adsorbents including clinoptilolite [19], MCM-41 [20], organo-zeolite [36], goethite [37], and amorphous iron hydroxide [38]. The adsorption capacity obtained in this work was considerably higher than the previously studied adsorbents (Table 3).

4.2. Effect of contact time and kinetics of the adsorption process

To evaluate the kinetics of the adsorption process, the uptake of chromate was measured for different time intervals from 1 to 14 min (Fig. 8). The results showed that
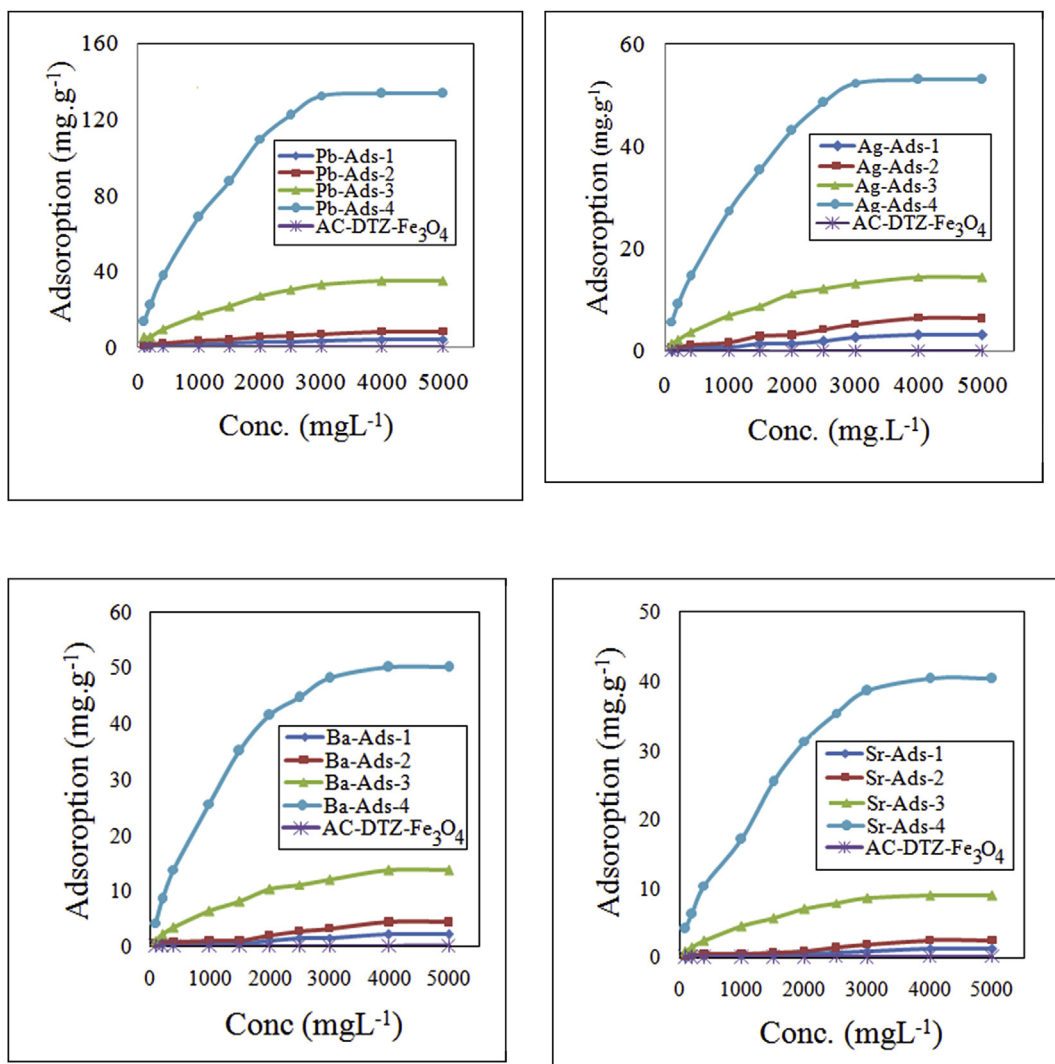
Fig. 7. Effect of chromate concentration on the chromate uptake.

Table 2
Removal of chromate by adsorbents with different cation loading.

Cation	Sample designation	k_{sp}	Adsorbed chromate (meq g^{-1})
Pb^{2+}	Pb-ads-1	2.8×10^{-13}	0.110
	Pb-ads-2		0.233
	Pb-ads-3		1.185
	Pb-ads-4		2.424
Ag^{+}	Ag-ads-1	1.1×10^{-12}	0.056
	Ag-ads-2		0.120
	Ag-ads-3		0.270
	Ag-ads-4		0.480
Ba^{2+}	Ba-ads-1	2.2×10^{-10}	0.038
	Ba-ads-2		0.118
	Ba-ads-3		0.432
	Ba-ads-4		0.946
Sr^{2+}	Sr-ads-1	2.2×10^{-05}	0.041
	Sr-ads-2		0.149
	Sr-ads-3		0.695
	Sr-ads-4		0.740

the adsorption process was kinetically fast and the equilibrium was established within 10 min. The kinetic data were analyzed using the pseudo-first-order and pseudo-second-order kinetic models.

The pseudo-first-order equation recommended by Lagergren and Sven [39] assumes that the sorption occurred on the sorption site of the adsorbent according to the following equation:

$$S_{(s)} + M^{n+}_{(aq)} \rightarrow SM^{n+} \tag{2}$$

where S is a sorption site on the adsorbent surface and M^{n+} is the ingoing species. The pseudo-first-order equation is expressed by the following equation:

$$\log(q_e - q_t) = \log q_e - \left(\frac{k_1}{2.303}\right) \tag{3}$$

where q_e and q_t are the amounts of the adsorbed ion (mg g^{-1}), respectively, at equilibrium and at time t, and k_1 is the Lagergren rate constant (min^{-1}). The value of k was determined by the plot of $\log(q_e - q_t)$ versus t (Fig. S3).

The pseudo-second-order equation can be visualized by Eq. (4):

$$S + M \underset{k''}{\overset{k'}{\rightleftarrows}} SM \qquad (4)$$

where S is the number of active sites occupied on the adsorbent, M is the concentration of free ions in the solution, SM is the concentration of metal ions bound to the sorbent, and k' and k'' are the adsorption and desorption rate constants, respectively.

The pseudo-second-order rate equation can be expressed by the following equations:

$$\frac{t}{q_t} = \frac{1}{(k_2 q_e^2)} + \left(\frac{1}{q_e}\right) t \qquad (5)$$

By plotting t/q_t versus t, a straight line was obtained (Fig. S4). The q_e and k_2 values were, respectively, obtained from the slope and intercept of the line.

According to the R^2 values obtained for the pseudo-first-order and pseudo-second-order equations (Fig. S3 and Fig. S4), it was concluded that the kinetic data were in good compliance with the pseudo-second-order model. In this regard, the following assumptions governed the adsorption process [40].

- Sorption only occurs on localized adsorption sites and involves no interaction between sorbed ions.
- The energy of adsorption is independent of surface coverage.
- Maximum adsorption corresponds to a saturated monolayer of adsorbate on the adsorbent surface.
- Chromate uptake is governed by the chemical process (chemisorption).
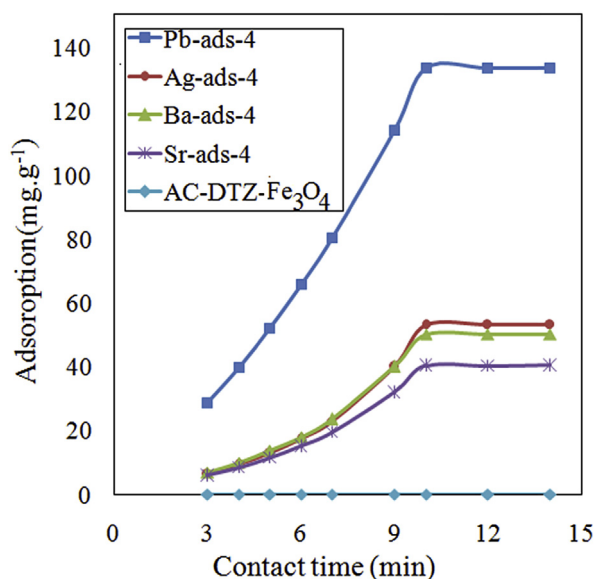- The rate-limiting step is a chemical sorption between the adsorbate and adsorbent.

Fig. 8. Effect of contact time on removal efficiency of chromate.

4.3. Effect of adsorbent dose on the chromate adsorption

To evaluate and optimize the effect of an adsorbent dose on the removal efficiency, the chromate uptake was measured with different adsorbent doses (0.1–2.6 g). The selected amount of the adsorbent was equilibrated with 25 mL of chromate solution (4000 $mg \cdot L^{-1}$). After equilibration, the adsorbent was separated and the concentration of chromate was measured in the remaining solution (Fig. 9). By Pb-Ads-4, 95% of removal efficiency was obtained with 0.4 g of the adsorbent, while; Sr-ADS-4 needed 2.2 g of the adsorbent for maximal removal efficiency.

M. Ghiaci et al. (2004) used natural zeolite clinoptilolite for the uptake of chromate from aqueous solutions. They reported that by an adsorbent dose of 4 g, the adsorption capacity of 4.53 $mg\,g^{-1}$ was achieved [21] while using 1.0 g of kaolinite the adsorption of 11.36 $mg\,g^{-1}$ was obtained. In
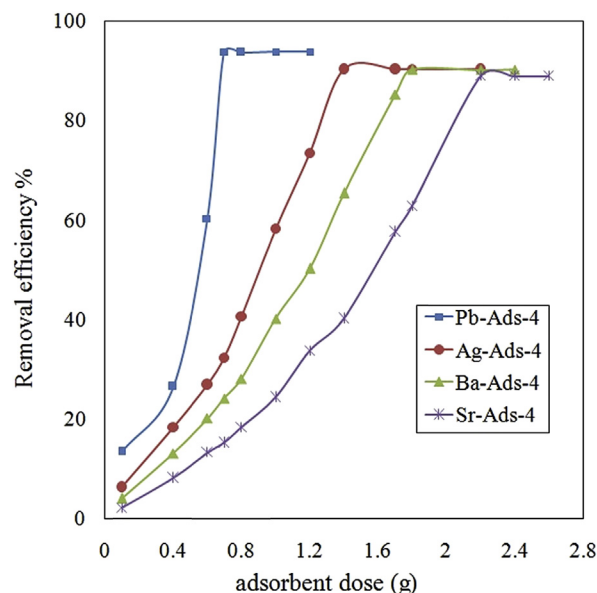
Table 3
Comparative sorption capacity of the previously studied adsorbents.

Adsorbent	Modified by	Conc. ($mg\,L^{-1}$)	Adsorption ($mg\,g^{-1}$)	References
Clinoptilolite	Ba^{2+}	70	84.5	[19]
	Pb^{2+}		105.6	
	Hg^{2+}		84.5	
	Ag^+		126.7	
	Sr^{2+}		73.9	
	Ca^{2+}		84.5	
Clinoptilolite	Without modification	139.2	45.36	[20]
Kaolinite	Hexadecyl trimethyl ammonium	10	11.36	[21]
Pillared clay	Hexadecyl trimethyl ammonium		8.10	
Organo-zeolite	Hexadecyltrimethylammonium	10	0.8	[36]
Goethite	—	58	—	[37]
Amorphous iron hydroxide	—	0.58	—	[38]
Magnetic activated carbon	Dithizone and Pb	4000	133.84	This work
	Dithizone and Ag		58.12	
	Dithizone and Ba		55.12	
	Dithizone and Sr		40.39	

Fig. 9. Effect of adsorbent dose on removal efficiency of chromate.

Fig. 10. Effect of pH on removal efficiency of chromate.

comparison with the previous studies, we achieved a higher adsorption capacity with a lower adsorbent dose.
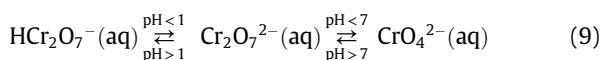
4.4. Effect of pH on the chromate adsorption

The pH of the solution, as an important factor in the adsorption process, by modifying the concentration of Cr(VI) species, changes the surface charge of the adsorbent, and H_3O^+ concentration. To evaluate the comprehensive effect of pH on the chromate uptake, the adsorption process was conducted at a pH range of 2–10. As shown in Fig. S5, at pHs lower than 5, the dominant species of Cr are $HCrO_4^-$, $Cr_2O_7^{2-}$, and H_2CrO_4 and the concentration of CrO_4^{2-} is negligible [41].

Therefore, the chromate uptake below pH=5.5 was very limited (Fig. 10). At higher pHs, the CrO_4^{2-} concentration begins to increase through the following reactions [42]:

$$Cr_2O_7^{2-} + H_2O \leftrightarrow 2HCrO_4^- \qquad (6)$$

$$H_2CrO_4^- \leftrightarrow HCrO_4^- + H^+ \qquad (7)$$

$$HCrO_4^- \leftrightarrow CrO_4^{2-} + H^+ \qquad (8)$$

and;

$$HCr_2O_7^-(aq) \underset{pH>1}{\overset{pH<1}{\rightleftharpoons}} Cr_2O_7^{2-}(aq) \underset{pH>7}{\overset{pH<7}{\rightleftharpoons}} CrO_4^{2-}(aq) \qquad (9)$$

The CrO_4^{2-} concentration increased as the pH of the solution increased and the maximum level was obtained at pH = 8. The uptake of CrO_4^{2-} followed the same pattern and the maximal removal was achieved at pH = 8 an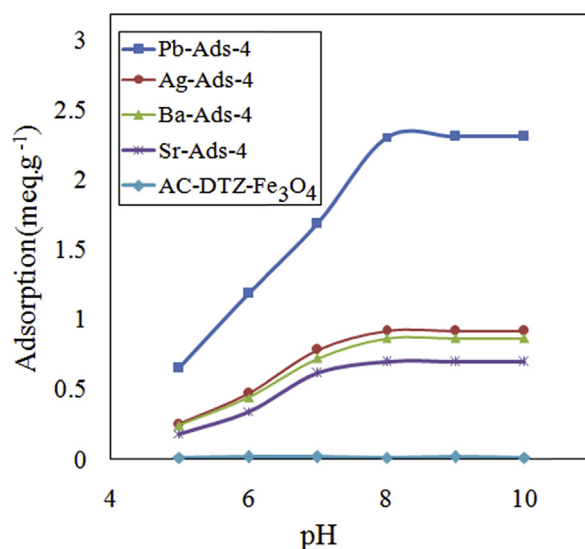d remained constant until pH = 10. To evaluate the effect of the surface charge of the adsorbent on the removal efficiency, the point of zero charge (pH_{pzc}) was measured by the use of five aliquots of sodium chloride solution (25 mL, 0.01 M) placing in contact with 0.1 g of the adsorbent. The system was stirred for 24 h, and the final pH was measured and plotted versus the initial pH (Fig. 11). It was concluded that the surface of the adsorbent was positive until pH = 8; therefore, the adsorbent surface did not exert a repulsion force to the CrO_4^{2-}.

The optimized pH for the removal of chromate was studied using different adsorbents including anion-exchange resins amberlite 416 [17], MCM-41 [20], and soil [43]. The optimized pH for the studied adsorbents was from 7 to 8, confirming that the chromate concentration and adsorbent surface charge are the most affecting parameters for the adsorption of chromate.

4.5. Selectivity of the adsorbents and effect of interfering anions

The interfering effect of various anions including OH^-, Cl^-, CO_3^{-2}, and NO_3^- was studied in the solution in which the concentration of chromate was constant (300 mg·L^{-1}), and the concentration of competing anions was progressively increased. The tolerance limit was defined as the concentration of coexisting anions that change the recovery of chromate within ±5%. The results of this experiment (Table 4) revealed that the interfering effect imposed by the studied anions followed the order of Sr-ads-4 > Ba-ads-4 > Ag-ads-4 > Pb-ads-4. These results confirmed that with smaller k_{sp}, the formation of the chromate precipitate with the loaded cation increased and the effect of interfering anions decreased. Among the studied anions, nitrate and CO_3^{-2} had, respectively, the lowest and highest interfering effects. The high interfering effect of CO_3^{-2} is attributed to the ability of the loaded cations to form an insoluble precipitate with CO_3^{-2}.
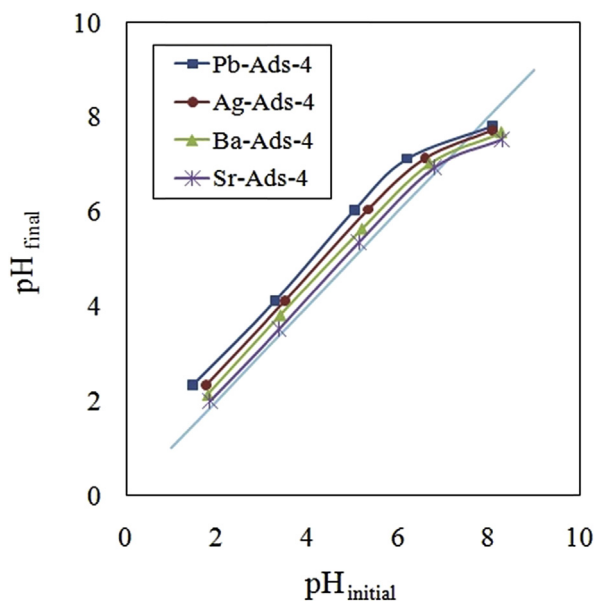
Fig. 11. pH$_{pzc}$ of the adsorbents.

Fig. 12. Effect of ionic strength on chromate removal.

Table 4
Tolerance limit of the studied interfering ions.

Interfering ion	Conc. (mg L^{-1})	%Recovery			
		Pb^{2+}	Ag$^+$	Ba^{2+}	Sr^{2+}
OH$^-$	0	99.9	99.8	99.1	98.7
	100	99.5	99.6	98.9	98.5
	200	98.8	98.1	97.9	97.4
	300	97.5	97.1	94.1	94.3
	400	90.1	90	88.2	88.5
Cl$^-$	0	99.9	99.8	99.1	98.7
	100	99.4	99.7	98.5	98
	200	98.1	97.6	96.4	97
	300	96.5	96.1	89.8	90.1
	400	89.2	89	87.4	87.9
CO$_3^{-2}$	0	99.9	99.8	99.1	98.7
	50	98.7	98.8	97.3	97.1
	100	96.3	97.8	95.7	95.5
	200	93.6	92.1	89.1	90.5
NO$_3^-$	0	99.9	99.8	99.1	98.7
	100	99.8	99.6	98.1	98.3
	200	98.6	98.7	97.8	97.4
	400	97.3	97.6	93.8	93.1
	500	94.1	94.5	89.8	90.8

4.6. Effect of ionic strength

To examine the effect of ionic strength of the solution on the uptake of chromate, the adsorption experiments in the solution in which the adsorbents were equilibrated with chromate solution (300 mg L^{-1}) in the presence of varying concentrations of NaCl (0.01, 0.05, and 0.1 mol L^{-1}).

Based on the obtained results, the adsorption of chromate decreased with an increase in the ionic strength of the solution (Fig. 12). The effect was more pronounced at ionic strengths higher than 0.5 mol L^{-1}. It is assumed that the well-known "electrolyte effect" reduced the affinity of the chromate anions for precipitation with the loaded cations
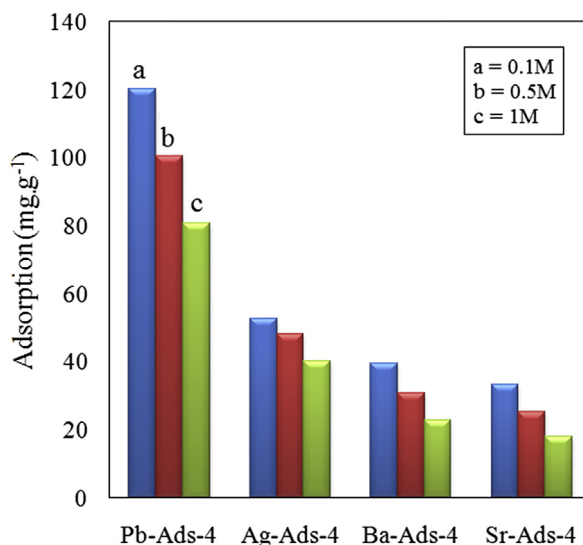
leading to lower chromate uptake. The effect of ionic strength on the sorption of chromate by iron and aluminum hydroxides indicated that in the presence of 0.1 M NaCl, the adsorption reduced to 90% of its initial value [44]. A similar observation was made for the adsorption of chromate by using vermiculite pure clay mineral [45]. The chromate uptake by using a surfactant-modified zeolite was significantly decreased with an increase in the ionic strength of the solution [46].

5. Desorption of chromate

The attempts to desorb CrO$_4^{2-}$ from the loaded adsorbent by the use of deionized water at pHs lower than 5.0 did not lead to the significant recovery of chromate because the solubility of the chromate precipitate is limited at lower pH values. Therefore, the chromate loaded on the biosorbent was eluted with 25 mL of a 0.1 M NaOH solution. The desorption ratios were calculated according to the following equation:

$$Recovery\% = \frac{mg \ of \ desorbed \ chromate}{mg \ of \ initially \ adsorbed \ chromate} \times 100$$

(10)

The desorption of chromate was between 79 and 87%. The highest value of recovery was observed for Sr-ads-4 and the lowest by Pb-ads-4 (Fig. 13). It seems that the regeneration depended on the k_{sp} of the chromate precipitate such that a small k_{sp} resulted in a lower recovery percentage.

6. Adsorption isotherms

In this work, the Langmuir, Freundlich, Redlich–Peterson, and Sips isotherm models were used to describe the adsorption of chromate by the adsorbents [47].
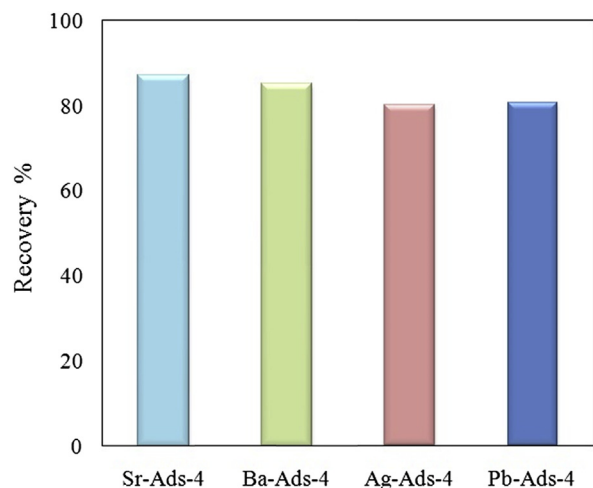
Fig. 13. Recovery of chromate from adsorbent by elution with NaOH.

Table 5
Langmuir, Freundlich, Redlich–Peterson, and Sips isotherm parameters.

Isotherm	Parameter	Adsorbents			
		Pb-ads-4	Ag-ads-4	Ba-ads-4	Sr-ads-4
Langmuir	K_L (L mg^{-1})	0.00061	0.000586	0.0005	0.00059
	q_m (mg g^{-1})	200	66.6	71.4	55.5
	R^2	0.999	0.999	0.999	0.999
	ARE	0.06	0.76	0.026	0.032
	EABS	60.9	224.8	6.7	7.08
Freundlich	K_F (L mg^{-1})	0.93	0.84	0.211	0.212
	n	1. 61	1.93	1.462	1.541
	R^2	0.979	0.973	0.989	0.994
	ARE	0.09	0.87	0.97	0.97
	EABS	70.16	257	264.6	217.4
Redlich–Peterson	A	0.22	0.09	0.06	0.09
	B	0.0482	0.0438	0.02	0.138
	g	0.553	0.569	0.608	0.473
	R^2	0.993	0.991	0.974	0.988
	ARE	0.904	0.89	0.53	0.92
	EABS	694.3	278.2	56.3	137.3
Sips	K_s (L mg^{-1})	0.00088	0.00092	0.00063	0.00011
	Q_{max} (mg g^{-1})	166.6	58.82	71.4	38.46
	m	1	1	1	1
	R^2	0.990	0.992	0.998	0.995
	ARE	0.086	0.93	6.12	0.98
	EABS	58.8	279.9	232.7	141.5

Among them, the Langmuir and Freundlich models are the most conventional mathematical models which can describe the amount of adsorbed cations distributed between the solution and the adsorbent. The Sips and Redlich–Peterson isotherms are a combination of the Langmuir and Freundlich isotherms. The isotherms are briefly explained as follows:

6.1. Langmuir isotherm

The Langmuir isotherm describing the monolayer adsorption of adsorbate on the surface of sorbent is based on the following assumption:

- the adsorption sites are homogeneously distributed on the surface of the adsorbent;
- the number of adsorbed species does not exceed the total adsorption sites; or the adsorption is limited to the formation of a monolayer;
- the adsorption sites have similar energy and similar affinity towards the adsorbates;
- no solute–solute or solute–solvent interaction in either phase occurs and both surface and bulk phases exhibit ideal.

The Langmuir model can be described by the following equation:

$$\frac{C_e}{q_e} = \frac{C_e}{q_m} + \frac{1}{b\,q_m\mathrm{m}} \tag{11}$$

where C_e is the equilibrium concentration (mg L^{-1}), q_e is the equilibrium adsorption capacity (mg g^{-1}), and b is the Langmuir constant related to the energy of adsorption, q_m (mg g^{-1}) is the maximum amount of the adsorbate to form a monolayer adsorption. By plotting C_e/q versus C_e, a straight line was obtained (Fig. S6), and the values of q were calculated from the slopes ($1/q_m$) and intercepts of the line [$1/(q_m K_L)$] and given in Table 5. As indicated in Fig. S6 and

Table 5, the adsorption data of different adsorbents (Pb-ads-4, Ag-ads-4, Ba-ads-4 and Sr-ads-4) analyzed using the Langmuir model produced the R^2 values of 0.999, which was higher than the values obtained for the other studied models. Therefore, the assumption that the adsorbent surface was homogeneous and the adsorption of each species on the surface had equal activation energy was confirmed.

6.2. Freundlich isotherm

The Freundlich model describes the adsorption that occurs on the heterogeneous surface with a multilayer and non-uniform adsorption process. The Freundlich isotherm can be defined by the following equation:

$$\log q_e = \log k_f + \frac{1}{n}\log C_e \tag{12}$$

where C_e is the equilibrium concentration (mg L^{-1}), q_e is the amount of species adsorbed per unit mass of the adsorbent at equilibrium (mg g^{-1}), and k_f and n are Freundlich constants related to adsorption capacity and adsorption intensity. By plotting $\log q_e$ versus $\log C_e$, a straight line was obtained and the Freundlich constants (n and k_f) were, respectively, calculated from the slope and the intercept of the line (Fig. S6). The results are given in Table 5. The R^2 values of 0.979, 0.973, 0.989, and 0.994 were, respectively, obtained for Pb-ads-4, Ag-ads-4, Ba-ads-4 and Sr-ads-4, which are lower than the values obtained for the Langmuir isotherms. Since the R^2 indicated the goodness-of-fit of experimental data on the isotherms models, this was evident that the experimental data were fitted logically to the Langmuir isotherm model describing that the surface of the functionalized adsorbent was homogeneous and a monolayer adsorption took place.

6.3. The Redlich-Peterson isotherm

The Redlich–Peterson isotherm contains the three parameters *A, B,* and *g,* which include features of the Langmuir and Freundlich isotherms. The Redlich–Peterson isotherm model can be described mathematically by the following equation:

$$\ln\left(A\frac{C_e}{q_e} - 1\right) = g\ln(C_e) + \ln(B) \tag{13}$$

C_e is the equilibrium concentration (mg L^{-1}) and q_e is the equilibrium adsorption capacity (mg g^{-1}). A plot of ln $(C_e/q_e - 1)$ versus ln (C_e) gives a straight line, where *A, B,* and *g* are evaluated from the plot (Fig. S6). The value of *g* lies between 0 and 1. When $g = 1$, the equation become the Langmuir equation [48]. When $g = 0$, it is closer to the Freundlich equation [49]. However, the accuracy of these interpretations strongly depends on the fitting method. When $A = 0$, it corresponds to the Freundlich model.

A values of 0.22, 0.09, 0.05, and 0.09 were, respectively, obtained for Pb-ads-4, Ba-ads-4, and Sr-ads-4, respectively, based on the results, since the values of *A* are not zero, so the experimental data obeyed the Langmuir isotherm. The *g* values of 0.553, 0.569, 0.608, and 0.473 obtained, respectively, for Pb-ads-4, Ag-ads-4, Ba-ads-4, and Sr-ads-4, which were closer to 1, also are the evidence of the fitness of data to the Langmuir isotherm (Table 5). By investigation on the Redlich parameters, and considering the calculated parameters (*g* and *A*), more evidence was obtained to confirm that the data were fitted to the Langmuir isotherm model.

6.4. Sips isotherm

The Sips isotherm is a combination of the Langmuir and Freundlich isotherms, this system explains that adsorbed molecules could occupy more than one adsorption site [48]. At low concentrations, the sips model reduces to the Freundlich isotherm while at high concentrations, it resembles to the Langmuir isotherm [50]. Sips isotherm is explained using the following equation:

$$\frac{1}{q_e} = \frac{1}{Q_{max}K_s}\left(\frac{1}{C_e}\right)^{1/m} + \left(\frac{1}{Q_{max}}\right) \tag{14}$$

where Q_{max} is the maximum adsorption capacity (mg g^{-1}) and K_S and *m* are, respectively, the Sips equilibrium constant (L mg^{-1}) and model exponent constant (Table 5).

The Sips isotherm describes the heterogeneity of the system, if m is between 0 and 1. When $m = 1$, the Sips equation resembles to the Langmuir equation, which confirms a homogeneous adsorption process. The isotherm parameters can be calculated from the plot of $1/q_e$ versus $1/C_e$ (Fig. S6). The value of *m* for Pb-ads-4, Ag-ads-4, Ba-ads-4, and Sr-ads-4 was 1 (Table 5).

In order to determine the fitness of the applied model to the experimental data, three factors were considered.

- The value of R^2 obtained for the Langmuir isotherm was closer to 1 than the value obtained for the Freundlich isotherm.
- The value of m in the Sips model was close to 1, so it resembles the Langmuir equation.
- The value of *A* obtained for the Redlich–Peterson isotherm was not zero, confirming that the data were in agreement with the Langmuir model.

7. Error analysis

The R^2 value, which indicates the difference between experimental and theoretical values, is restricted only in linearized plots. Therefore, in order to determine the fitness of applied models to the experimental data, the error analysis is required to analyze the data. In this work, the error analysis was performed by two different error functions including average relative error (ARE) and sum of the absolute errors (EABS) (Table 5).

7.1. Average relative error (ARE)

This error function is applied to minimize the fractional error distribution across the entire concentration range [49,50]. This method is based on the following equations:

$$\text{ARE} = \frac{\sum |(q_c - q_e)/q_e|}{n} \tag{15}$$

where q_c and q_e are respectively the equilibrium and experimental adsorption capacity (mg g^{-1}), and *n* is the number of experimental data.

7.2. Sum of the absolute errors (EABS)

The isotherm model parameters determined by using the EABS function provide a better fit as the magnitudes of the errors increase [51]. The EABS is described using the following equation:

$$\text{EABS} = \sum |q_{exp} - q_{cal}| \tag{16}$$

The isotherms with smaller errors are more acceptable. According to the results given in Table 5, the error analysis also confirmed that the Langmuir model was the most reliable isotherm to explain the experimental data.

Based on the Langmuir model, adsorption was a monolayer, all sites were identical and energetically equivalent, the adsorption energy was constant, there was no interaction between species adsorbed on neighboring sites, and the adsorbent has a finite capacity [52].

8. Effect of temperature and thermodynamic parameters

The influence of temperature on the adsorption process was evaluated by the thermodynamic parameters calculated by the following equations:

Table 6
Thermodynamics adsorption parameters.

Sample	ΔH^o (J mol^{-1})	ΔS^o (J mol^{-1})	ΔG^o (kJ mol^{-1}) at 25°C
Pb-ads-4	−7.78	−0.490	−0.14
Ag-ads-4	−5.42	−16.5	−4.91
Ba-ads-4	−5.34	−17.7	−5.26
Sr-ads-4	−3.17	−27.7	−8.25

$$K_d = \frac{C_i - C_e}{C_e} \times \frac{V}{M} \tag{17}$$

$$\ln K_d = \left(\frac{\Delta S^\circ}{R}\right) - \left(\frac{\Delta H^\circ}{RT}\right) \tag{18}$$

$$\Delta G = -RT \ln K_d \tag{19}$$

where K_d is the distribution coefficient, C_o is initial concentration ingoing ion (mg L^{-1}), C_e is the equilibrium concentration (mg L^{-1}), V (L) is the volume of the solution, and m (g) is the mass of adsorbent. ΔG° is the Gibbs free energy, ΔH^o is the change in enthalpy (J mol^{-1}), and ΔS^o is the entropy changes of the reaction (J mol^{-1} K^{-1}). R is the gas constant (8.3144 J K mol^{-1}) and T (K) is the temperature. The thermodynamic studies were studied at four temperatures of 25, 30, 35, and 40 °C. By plotting $\ln k_d$ versus $1/T$, the ΔH° and ΔS° parameters can be obtained, respectively, from the slope and intercepts of the Van't Hoff plot (Fig. S7).The slope and intercept of the line are equal to $(-\Delta H^\circ/R)$ and $(\Delta S^\circ/R)$, respectively. The negative value of ΔG° demonstrated that the adsorption process was spontaneous. As temperature rises, the adsorption process became more favorable. The positive value of enthalpy and entropy suggests the endothermic nature and a random increase in the adsorption process, respectively (Table 6).

9. Conclusion

The aim of this research was to study the adsorption performance of a new adsorbent synthesized using activated carbon prepared by oak-shell waste materials and impregnated with particular cations. The activated carbon was magnetized, modified with dithizone, and then impregnated with cations. In this study, adsorption capacities of 139.84, 58.12, 7.81, and 27 mg g^{-1} were obtained, respectively, for lead, silver, barium, and strontium, which were higher than the previously reported values. The adsorption capacity of the adsorbent impregnated with the studied cations toward the chromate anion was then measured under different experimental conditions. The results indicated that the uptake of chromate correlated with the number of loaded cations and the k_{sp} of the chromate precipitate. The adsorption process was kinetically fast and the equilibrium was established within 10 min. The used adsorbent was readily separated from the solution by applying an appropriate external magnetic field. The recovery of the adsorbent was performed by the use of NaOH solution, and most of its initial capacity was retained.

References

[1] I. Heidmann, W. Calmano, Separ. Purif. Technol. 61 (2008) 15−21.
[2] M.X. Loukidou, A.I. Zouboulis, T.D. Karapantsios, K.A. Matis, Colloids Surf A 242 (2004) 93−104.
[3] N.R. Axtell, S.P.K. Sternberg, K. Claussen, Bioresour. Technol. 89 (2003) 41−48.
[4] A.H. Mahvi, Int J Environ Sci Tech. 5 (2008) 275−285.
[5] US Environmental Protection Agency, Quality Criteria for Water:. EPA -440-5-86-001, U.S. Government Printing Office, Washington, 1986, 225 pp.
[6] Z.A. AL-Othman, R. Ali, M. Naushad, Chem. Eng. J. 184 (2012) 238−247.
[7] A.K. Golder, A.K. Chanda, A.N. Samanta, S. Ray, Separ. Purif. Technol. 76 (2011) 345−350.
[8] F. Gode, E. Pehlivan, J. Hazard Mater. 119 (2005) 175−182.
[9] L. Yurlova, A. Kryvoruchko, B. Kornilovich, Desalination 144 (2002) 255−260.
[10] S. Mukherjee, S. Mukhopadhyay, A. thuPariatamby, M.A. Hashim, G.B. Gupta, JTICE 53 (2015) 15−21.
[11] Y. Benito, M.L. Ruiz, Desalination 142 (2002) 229−234.
[12] N. Meunier, P. Drogui, C. Montané, R. Hausler, G. Mercier, J.F. Blais, J. Hazard. Mater. 137 (2006) 581−590.
[13] G. Qin, M.J. Mcguire, N.K. Blute, C. Seidel, L. Fong, Environ. Sci. Technol. 39 (2005) 6321−6327.
[14] D. Mohan, U. Charle, Pittman Jr., J. Hazard Mater. 137 (2006) 762−811.
[15] T.A. Kurniawan, G.Y.S. Chan, W.H. Lo, S. Babel, Chem. Eng. J. 118 (2006) 83−98.
[16] G.C. Panda, S.K. Das, T.S. Bandopadhyay, A.K. Guha, Colloids Surf. B Biointerfaces 57 (2007) 135−142.
[17] E. Korngold, N. Belayev, L. Aronov, Separ. Purif. Technol. 33 (2003) 179−187.
[18] M. Villalobos, A. Perez-Gallegos, J. Colloid Interface Sci. 326 (2008) 307−323.
[19] H. Faghihian, R.S. Bowman, Water Res. 39 (2005) 1099−1104.
[20] M. Ghiaci, R. Kiaa, A. Abbaspur, F. Seyedeyn-Azad, Separ. Purif. Technol. 40 (2004) 285−295.
[21] B.S. Krishna, D.S.R. Murty, B.S.J. Prakash, Appl. Clay Sci. 20 (2001) 65−71.
[22] C.H. Wu, S.L. Lo, C.F. Lin, Colloids Surf. A Phys. Eng. Aspect 166 (2000) 251−259.
[23] F. Hatami, H. Faghihian, Environ. Prog. 34 (2015) 1562−1567.
[24] S. Mokhtari, H. Faghihian, J.E.C.E 674 (2015) 1−7.
[25] M. Adibmehr, H. Faghihian, Chem. Eng. 205 (2018) 519−532.
[26] L.G. Djemmoe, T.E. Njanja, M.C.N. Deussi, K.I. Tonle, C. R. Chimie (2016) 1−9.
[27] B. Volesky, Sorption and Biosorption, BV-Sorbex, Inc, Quebec, Canada, 2003.
[28] Z. Jiang, Y. Lin, X. Sun, F. Tain, F. Sun, C. Liang, W. You, C. Han, C. Li, Langmuir 19 (2003) 731−736.
[29] P. Panneerselvam, N. Morad, K.A. Tan, J. Hazard Mater. 186 (2011) 160−168.
[30] J. Yu, R. Chi, Y. Zhang, Zh. Xu, Ch. Xiao, J. Guo, Bioresour. Technol. 110 (2012) 160−166.
[31] J. Zhou, G. Zhao, J. Yang, G. Han, J. Alloy. Comp. 509 (2011) 6731−6735.
[32] M. Chahud, M.A.S.C. Filho, N.S. Fernandes, M.I. shiro, Eclet Quím. 25 (2000) 1−6.
[33] Z.L. Chen, Y. Sun, P. Huang, X.X. Yang, X.P. Zhou, Nanoscale Res. Lett. 4 (2009) 400−408.

[34] H. Wang, X. Xu, Zh. Ren, B. Gaom, RSC Adv. 6 (2016) 47237–47248.
[35] Zh. Wang, H. Guo, F. She, G. Yang, Y. Zhang, Y. Zeng, L. Wang, H. Xiao, S. Deng, Chemosphere 119 (2015) 646–653.
[36] G.M. Haggerty, R.S. Bowman, Environ. Sci. Technol. 28 (1994) 452–458.
[37] C.C. Ainsworth, D.C. Girvin, J.M. Zachara, S.C. Smith, Soil Sci. Soc. Am. J. 53 (1989) 411–418.
[38] J. Zachara, D. Girvln, R. Schmidt, Environ. Sci. Technol. 21 (1907) 589–594.
[39] S. Lagergren, K. Sven, K.vet.Akad. handl. 24 (1898) 1–39.
[40] D. Mohan, U. Charles, Pittman Jr., M. Bricka, F. Smith, B. Yancey, J. Mohammad, P.H. Steele, A.M.F. lexandre-Franco, V. Gómez-Serrano, H. Gong, J. Colloid Interface Sci. 310 (2007) 57–73.
[41] B. Karabacakoğlu, Ö. Savlak, Ind. Eng. Chem. Res. 53 (2014) 13171–21379.
[42] F.A. Cotton, G. Wilkinson, Advanced Inorganic Chemistry, Wiley, New York, 1988.
[43] J.M. Zachara, C.C. Ainsworth, C.E. Cowan, C.T. Resch, Soil Sci. Soc. Am. J. 53 (1989) 418–428.
[44] O. Ajouyed, C. Hure, M. Ammari, L. BenAllal, N. Marmier, J. Hazard Mater. 174 (2010) 616–622.
[45] A.A. El-Bayaa, N.A. Badawy, E.A. AKhalik, J. Hazard Mater. 170 (2009) 1204–1209.
[46] L. Zhaohui, J. Environ. Eng. 130 (2004) 205–208.
[47] L.V. Gurgel, L.F. Gil, Water Res. 43 (2009) 4479–4488.
[48] M. Brdar, M. Sciban, A. Takaci, T. Dosenovic, Chem. Eng. J. 183 (2012) 108–111.
[49] T.R.N. Kumara, N. Hamdan, M. IskandarPetra, K.U. Tennakoon, P. Ekanayake, J. Chem. 468975 (2014) 1–6.
[50] E. Simsek, U. Beker, Kor. J. Chem. Eng. 31 (2014) 2057–2069.
[51] L.S. Chan, W.H. Cheung, S.J. Alle, G. McKay, Chin. J. Chem. Eng. 20 (2012) 535–542.
[52] H. Shahbeig, N. Bagheri, S.A. Ghorbanian, A. Hallajisani, S. Poorkarimi, WJ MS 9 (2013) 243–254.